CHEMISTRY OF MATERIALS

ARTICLE

pubs.acs.org/cm

Synthesis of Single-Crystal-Like, Hierarchically Nanoporous Silica and Periodic Mesoporous Organosilica, Using Polyelectrolyte−Surfactant Mesomorphous Complexes as a Template

Na Li, Jin-Gui Wang, Hui-Jing Zhou, Ping-Chuan Sun, and Tie-Hong Chen*

Institute of New Catalytic Materials Science, Key Laboratory of Advanced Energy Materials Chemistry (MOE), College of Chemistry, Nankai University, Tianjin 300071, People's Republic of China

Supporting Information

ABSTRACT: Single-crystal-like, hierarchically nanoporous silica SBA-1 particles were successfully fabricated by employing organic mesomorphous complexes of polyelectrolyte (poly(acrylic acid) (PAA)) and cationic surfactant (hexadecylpyridinium chloride (CPC)) as templates. By adjusting the amount of PAA in the synthesis, a series of silica particles with well-defined morphologies and well-ordered cubic $Pm\bar{3}n$ mesostructure were obtained. Both the mesostructure and well-defined morphology of the silica particles inherited those of the corresponding PAA/CPC mesomorphous complexes. The materials possess bimodal nanopores corresponding to the mesopore size of SBA-1 templated by surfactant micelles and secondary interstitial nanopores templated by phase-separated PAA with different domain sizes, respectively. Notably, the presence of a large amount of foamlike secondary nanopores did not disturb the single-crystal characteristic of the SBA-1 particles. By means of pore-expanding with 1,3,5-trimethylbenzene, the mesopore size of the SBA-1 could be easily tuned from 3.0 nm to 5.0 nm, and the secondary nanopore were enlarged to several hundreds of nanometers, while the morphology of the particles was not changed. Besides, using bridged organosilane as a precursor, a series of hierarchically nanoporous periodic mesoporous organosilicas (H-PMO) with well-defined morphology were fabricated. Because of the hierarchically nanoporous structure and inherent hydrophobic bridged-ethylene group, the H-PMO exhibited rapid adsorption rate and high adsorption capacity in enzyme and protein immobilization.

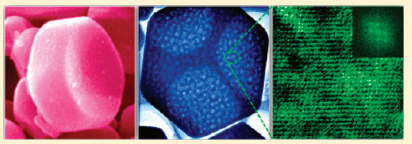

KEYWORDS: polyelectrolyte, surfactant, mesomorphous, nanoporous, periodic mesoporous organosilicas, single-crystal-like

INTRODUCTION

Hierarchically porous materials with well-defined morphologies have been of growing interest, because of their potential applications in catalysis, adsorption, separation, and biomedical systems. In the past decades, a variety of templating approaches have been proposed to synthesize hierarchically porous materials, and colloidal particles, polymers, emulsion droplets, and surfactants have been employed to create porous structures with different sizes. Bimodal or trimodal porous materials, including micromeso, meso−meso, meso−macro, and even micromeso−macro, have been reported.[1−6] However, in most cases, the control of well-ordered mesostructure and well-defined morphology was difficult, because of the mixing of different types of templates in the syntheses. In contrast, some natural biominerals (for instance, sea urchin spines) possess complex and spongelike morphology but still remain single crystalline.[7] The formation mechanism of the "porous" single crystals of biominerals can be ascribed to a time-dependent cooperative organization with complex organic matrix as dynamic templates.[8]

It is well-known that ionic self-assembly of polyelectrolyte and oppositely charged surfactants could form highly ordered mesomorphous phases;[9] however, the organic complexes were rarely utilized as templates in the synthesis of mesoporous materials.[10] In a recent communication,[11] we first introduced the synthesis of hollow carved single-crystal mesoporous silica spheres, using the mesomorphous complex of poly(acrylic acid) (PAA) and cetyltrimethylammonium bromide (CTAB) as dynamic templates. With the addition of silane to the suspension of colloidal particles of PAA/CTAB mesomorphous complex, the silica precursors formed after silane hydrolysis co-assembled with CTAB micelles to form mesostructured silica; meanwhile, PAA chains were extruded and phase-separated from the PAA/CTAB complex and served as a template for interstitial nanopores. Interestingly and importantly, the presence of a large amount of secondary nanopores did not disturb the single-crystal mesostructure of the mesoporous silica particles, which would possess both the functions of crystal-like regularity and high diffusion efficiency of hierarchical pores.

In recent years, periodic mesoporous organosilicas (PMO), defined as a new class of organic−inorganic hybrid materials with the organic fragments regularly distributed in the framework, have attracted significant interest.[12] Because of the highly ordered structure with tunable pore size, and high hydrothermal and mechanical stability, as well as the organic moiety in the pore wall, the PMO materials were favorable for the immobilization of enzymes and proteins.[13] However, most PMO materials possessed a single porous structure and were limited in applications if a rapid diffusion rate, as well as higher activity and selectivity, were required. Zhou et al. reported the synthesis of a series of

Received: June 22, 2011
Revised: August 3, 2011
Published: August 23, 2011

PMO materials with bimodal cagelike pores and the hybrid nature, as well as the hierarchical structure of these materials, made them superior enzyme supports.[14] Ordered mesoporous materials with intrinsic high specific surface area, as well as regular and tunable pore size, have been regarded as promising adsorbents in bioadsorption and separation.[15] Thus, the synthesis of hierarchically nanoporous PMO materials with well-ordered structure and well-defined morphology is urgently needed for bioimmobilization.

In the present study, single-crystal-like, hierarchically nanoporous silica SBA-1 with well-defined morphology was synthesized with anionic polymer PAA and cationic surfactant hexadecylpyridinium chloride (CPC) mesomorphous complexes as templates. By means of pore-expanding with 1,3,5-trimethylbenzene, the mesopore size of the SBA-1 could be easily tuned from 3.0 nm to 5.0 nm, while the morphology of the particles was not changed. Moreover, hierarchically nanoporous PMO were also prepared by employing bridged silsesquioxane species $(RO)_3Si-CH_2-CH_2-Si(RO)_3$ as a precursor. To the best of our knowledge, there are no reports on PMO materials possessing a hierarchically porous structure with single-crystal-like morphology. Because of the hierarchical nanoporous structure and the inherent hydrophobic bridged-ethylene groups, the H-PMO exhibited a rapid adsorption rate and high adsorption capacity in enzyme and protein immobilization.

EXPERIMENTAL SECTION

Chemicals. Hexadecylpyridinium chloride (CPC) and 1,3,5-trimethylbenzene (TMB) were obtained from Aladdin, China. Poly(acrylic acid) (PAA) (average molecular weight = 240 000, 25% solution in water) was obtained from Acros. In this work, the amount of PAA used in the synthesis means the weight of the 25% solution. 1,2-Bis(triethoxysilyl)ethane $((C_2H_5O)_3SiCH_2CH_2Si(OC_2H_5)_3$, referenced hereafter as BTEE; 96% purity) was obtained from Fluorochem Limited. Lysozyme and bovine serum albumin (BSA) were obtained from Sigma−Aldrich. All the chemical agents were used without further purification.

Synthesis of Hierarchically Nanoporous SBA-1. In a typical synthesis, 0.54 g of CPC was dissolved in 25.0 g of deionized water under stirring, and a certain amount (4−7.5 g) of PAA solution was added under vigorous stirring at room temperature to obtain a clear solution. Next, 4.0 g of ammonia solution (25%) was added to the above solution under vigorous stirring and the solution became a milky suspension, because of the formation of PAA/CPC complex particles. After further stirring for 20 min, 2.08 g of tetraethylsiloxane (TEOS) was added to the above suspension. The mixture was stirred for another 15 min, and then was transferred to an autoclave, which was placed in an oven at 80 °C for 48 h. The final product was centrifugated, washed with deionized water, and dried at 60 °C. The organic templates were removed by calcination at 550 °C for 5 h. The samples were denoted as SBA-1-*x* (where the suffix number *x* indicates the amount of PAA used in the synthesis).

Incorporation of 1,3,5-TMB as Pore-Swelling Agents. The incorporation of 1,3,5-TMB as a pore-swelling agent was carried out using a procedure similar to that described above, with the amount of PAA being 7.5 g. After the addition of ammonia solution, different amounts of 1,3,5-TMB (0.18−0.72 g) was subsequently added and stirred for 30 min. Then, 2.08 g of TEOS was added dropwisely into the above solution. After being stirred for 15 min, the mixture was put in an oven of 80 °C for 48 h. The final product was centrifugated, washed, dried, and calcined at 550 °C for 5 h. The samples were denoted as SBA-1-TMB-*x* (where the suffix number *x* indicates the amount of TMB used in the synthesis).

Synthesis of Hierarchically Nanoporous Periodic Mesoporous Organosilicas (H-PMO). In brief, after mixing 0.54 g of CPC, 25 mL of H_2O, 7.5 g of PAA, 4.0 g of ammonia solution with vigorous stirring, and 1.8−3.6 g of BTEE were added. The mixture was stirred for 20 min, and then conducted under static conditions for 48 h at room temperature. The final product was centrifugated, dried, and calcined. The organic templates were removed by a Soxhlet extraction in 100 mL of ethanol with 5 mL of 36% HCl aqueous solution for 2 days. The samples were denoted as H-PMO-*x* (where the suffix number *x* indicates the amount of BTEE used in the synthesis).

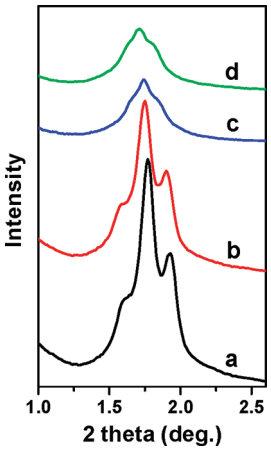

Figure 1. Small-angle X-ray scattering (SAXS) patterns of the calcined SBA-1 samples obtained with different amounts of PAA (4 g (pattern a), 5 g (pattern b), 6 g (pattern c), and 7.5 g (pattern d)).

Synthesis of MCM-41 and SBA-15. MCM-41 and SBA-15 was prepared using the methods reported in the literature, respectively.[16] The preparation of MCM-41 involves the following: 0.85 g of CTAB was dissolved in a mixture of 200 g of water and 14.3 g of ammonium hydroxide. Then, 4.37 g of TEOS was added to this homogeneous solution with vigorous stirring for 10 min and then heated at 80 °C for 2 h. The preparation of SBA-15 first involves the the dissolution of 2 g of P123 in 15 mL of H_2O, followed by the addition of 30 g of 2 M HCl solution and the dropwise addition of 4.3 g of TEOS. The mixture was stirred at 30 °C for 24 h, after which it was placed in an oven of 80 °C for 24 h.

Lysozyme Immobilization. Approximately 5 mg of the silica sample was dispersed in 5 mL of lysozyme stock solution with a concentration of 0.5 mg mL^{-1} in 50 mM PB at pH 7.0. The suspensions were separated by centrifugation at 8000 rpm for 5 min and then washed twice with 5 mL of 50 mM PB. The supernatants of the lysozyme solution were collected. Lysozyme concentrations were determined using the characteristic ultraviolet−visible light (UV−vis) absorbance of lysozyme at 280 nm. The difference in the lysozyme amount in solution before and after adsorption was deemed equal to the amount of lysozyme adsorbed on the material.

Bovine Serum Albumin (BSA) Adsorption. The adsorption of bovine serum albumin (BSA) was carried out with the same method as the lysozyme. In a typical experiment, ~5 mg of the silica sample was dispersed in 5 mL of lysozyme stock solution with a concentration of 0.5 mg mL^{-1} in 10 mM acetate buffer at pH 4.7, and the resulting suspension was shaken at 25 °C for 24 h. After centrifugation and washing, the supernatants of the BSA solution were collected. Initial and final BSA concentrations were determined by a UV absorbance band at 280 nm.

Characterization. Small-angle X-ray scattering (SAXS) experiments were performed on a Bruker Nanostar small-angle X-ray scattering system. The X-ray diffraction (XRD) patterns were obtained on a Rigaku Model D/max-2500 diffractometer, with Cu Kα radiation at 40 kV and 100 mA. Scanning electron microscopy (SEM) images were obtained with a Shimadzu Model SS-550 instrument. Transmission

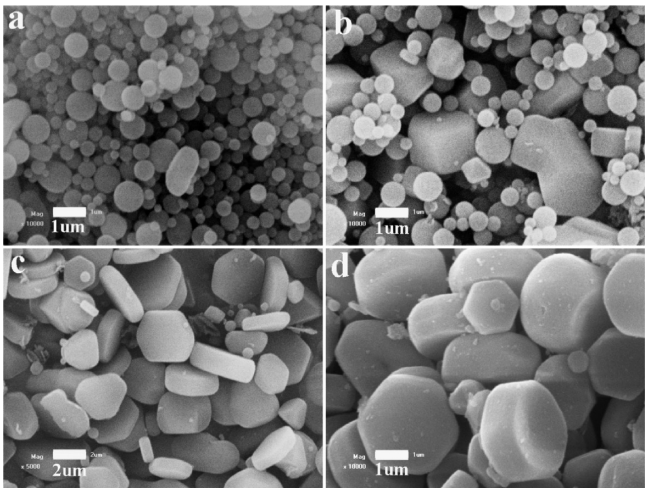

Figure 2. Scanning electron microscopy (SEM) images of the calcined SBA-1 samples obtained with differents amounts of PAA: (a) 4 g, (b) 5 g, (c) 6 g, and (d) 7.5 g.

electron microscopy (TEM) observations were performed on a Philips Model Tecnai F20 microscope, operating at 200 kV. All samples subjected to TEM measurements were dispersed in ethanol ultrasonically and were deposited dropwise onto copper grids. N_2 adsorption measurements were performed on a BELSORP-mini II sorption analyzer. The specific surface area was calculated using the Brunauer−Emmett−Teller (BET) method, the pore size distribution was calculated from the adsorption branch using the Barrett−Joyner−Halenda (BJH) method, and total pore volume was obtained at a relative pressure of p/p_0 = 0.99. Before measurements, the samples were dried under dry N_2 flow at 350 °C for 5 h. ^{13}C CP/MAS NMR spectra were measured with a spin rate of 12 kHz, a contact time of 0.8 ms, and a recycle delay of 3 s. UV−vis spectra were measured on a Shimadzu Model 2450 spectrometer.

RESULTS AND DISCUSSION

In our syntheses, the amount of CPC was kept constant and the amount of PAA was tuned to obtain a series of samples. Figure 1 shows the small-angle X-ray scattering (SAXS) patterns of the calcined samples. The SAXS patterns of the samples synthesized with 4 and 5 g of PAA exhibited three well-resolved diffraction peaks, which were indexed to the (200), (210), and (211) characteristic diffractions of the cubic $Pm\bar{3}n$ mesostructure of SBA-1. When the PAA was increased to 6 and 7.5 g, those three well-resolved diffraction peaks gradually became broadened and less-resolved, indicating the degraded long-range order of the mesostructure, and the reason for the less-ordered mesostructure, because of the addition of more PAA, will be discussed later in this paper.

The morphologies of the SBA-1 synthesized with different amounts of PAA were characterized by SEM, as shown in Figure 2. With the addition of 4 g of PAA, the sample was composed of submicrometer-sized spherical particles (see Figure 2a). If the PAA amount was increased to 5 g, some larger-sized polyhedral particles gradually appeared (Figure 2b). When the amount of PAA increased to 6 g and 7.5 g, micrometer-sized particles with uniform, well-defined morphology could be observed (see Figures 2c and 2d). The morphology of the particles was interesting, and some representative SEM images from different viewpoint are shown in Figure S1 in the Supporting Information. Generally, the morphology of the particles resembled a hexagonal

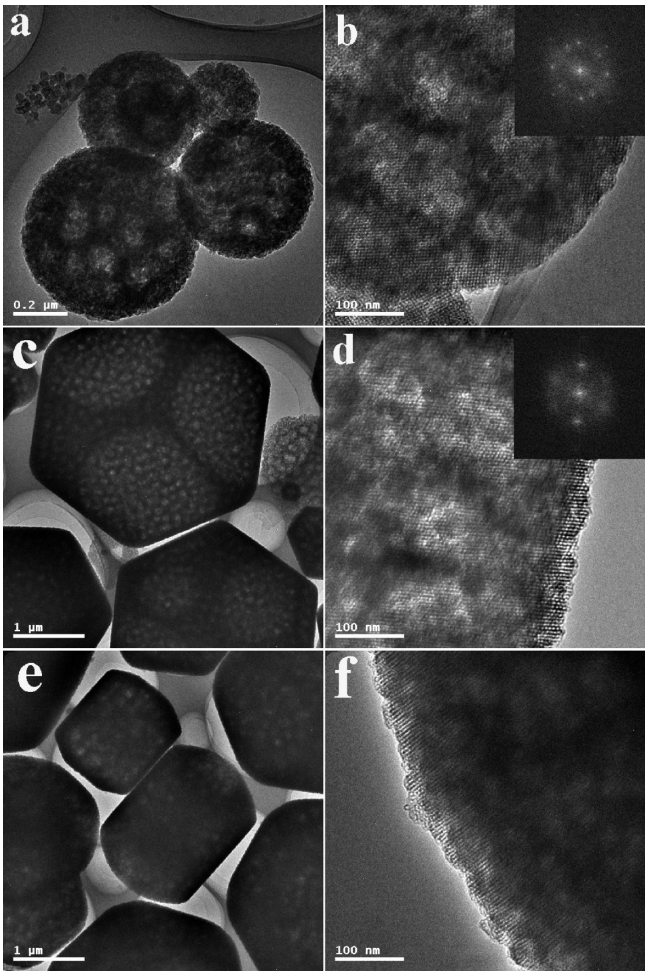

Figure 3. Transmission electron microscopy (TEM) images of calcined SBA-1 particles synthesized with different amounts of PAA: (a, b) 4 g and (c, d, e, f) 7.5 g. The insets in panels b and d are Fourier patterns.

prism but with truncated ends, and the hexagonal facade was not flat but somewhat concave. We would like to call the morphology of the particles a "drum-like polyhedron", and, depending on the thickness of the drum-like polyhedron, some thinner particles looked like moon cakes. Unusual morphologies such as hexagonal plates have been observed for silica mesoporous crystals with cubic $Fm\bar{3}m$ symmetry, and the morphology was explained by the presence of single twinning by the FCC crystal.[17] Accordingly, here, in our case, it may not be surprising that the particles displayed a hexagonal cross section for SBA-1 crystals with a cage-type cubic $Pm\bar{3}n$ symmetry.

Based on our results, obviously, the morphology and size of the SBA-1 particles were influenced by the amount of PAA in the synthesis. Without the addition of PAA, only irregular particles with two-dimensional hexagonal *p6mm* mesostructure were obtained, as shown in Figure S2 in the Supporting Information. With the addition of PAA in the synthesis, the electrostatic interaction between anionic PAA polymer chains and cationic surfactants would modify the surface charge and aggregation state of the surfactant micelles and induce the formation of complex salts with variation of mesophases.[9] In our synthesis, the anionic polymer PAA and cationic surfactant CPC self-assembled in ammonia solution and colloidal organic complex particles were formed before the addition of the silica precursor. The PAA/CPC complex colloidal particles prepared with different amounts of PAA

dx.doi.org/10.1021/cm2017856 |*Chem. Mater.* 2011, 23, 4241–4249

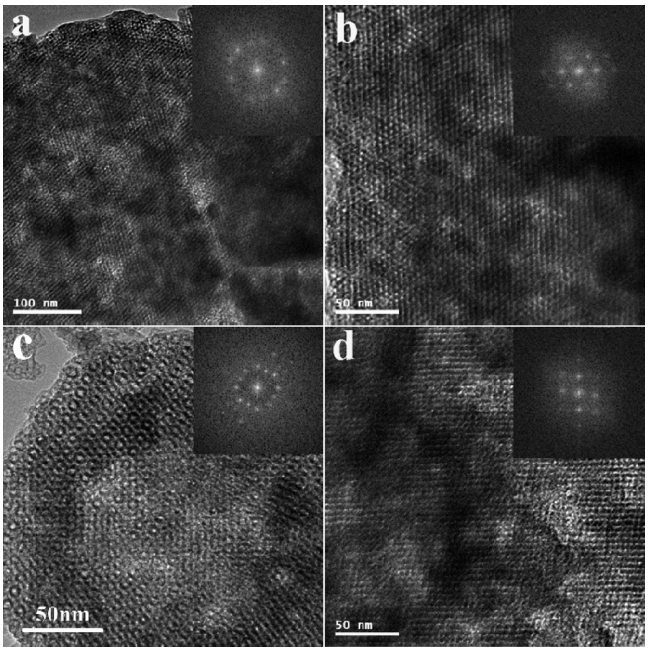

Figure 4. High-resolution TEM images along different directions and their Fourier patterns (insets) of the grinded calcined SBA-1 samples synthesized with 7.5 g of PAA. The observation direction in panel c is [100].

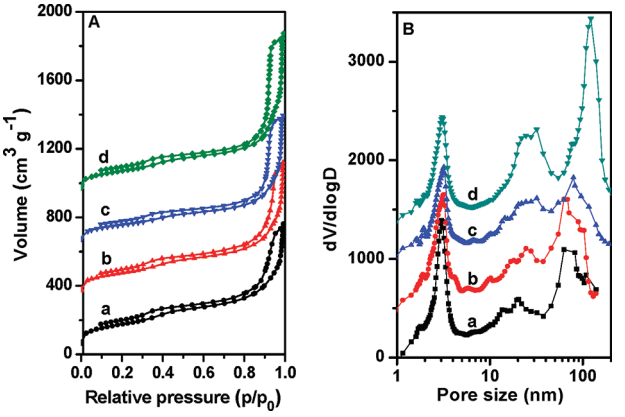

Figure 5. (A) Nitrogen adsorption−desorption isotherms and (B) pore size distribution curves of the calcined SBA-1 samples obtained with different amounts of PAA (4 g (curve a), 5 g (curve b), 6 g (curve c), and 7.5 g (curve d)). The pore size distribution of the samples was in the range of 2−200 nm; therefore, the curves are plotted on a logarithmic scale, for the sake of clarity.

(4 and 7.5 g, respectively) were prepared, obtained by centrifugation, and were subjected to SAXS and TEM measurements to monitor their mesophases and sizes. As shown in Figure S3 in the Supporting Information, the soft samples of PAA/CPC complexes exhibited mainly a cubic ordered $Pm\bar{3}n$ mesophase independent of the amount of PAA. It has been reported recently that the phase transition occurred in polyelectrolyte−surfactant complexes with different hydration states.[18] In the SAXS patterns of the PAA/CPC complex, some other mesophase also appeared and it was probably due to the drying of the soft sample during the measurement. TEM images of the PAA/CPC complexes (Figure S4 in the Supporting Information) indicated that the size of the complex particles increased with the amount of PAA. With 4 g of PAA, the size of the PAA/CPC complex particles was in the submicrometer range, whereas with 7.5 g of PAA, micrometer-sized complex particles were observed. It should be noted that, for TEM measurement, the PAA/CPC complex particles were deposited dropwise onto copper grids and dried, so the dried particles mainly exhibited the shape of irregular spheres (Figure S4 in the Supporting Information). However, occasionally, some particles with a hexagonal-shaped cross section could be observed in the TEM images (see panels c and d in Figure S4 in the Supporting Information). These results implied that both the mesostructure and well-defined morphology of the silica products inherited those of the corresponding PAA/CPC mesomorphous complexes. Note that the formation of mesostructured silica was not a simple replication of the mesophase and shape of the PAA/CPC complex; instead, the co-assembly between the silica precursors and the PAA/CPC complex would result in evolution of mesophase and morphology of the final mesostructure of silica.

In order to investigate the interior texture of the drumlike SBA-1 particles, the samples were grinded for SEM observation. As shown in Figure S5 in the Supporting Information, it is interesting to see that the interior of the SBA-1 particle exhibited foamlike features composed of interstitial nanopores. This indicated that the SBA-1 particles were hierarchically porous, as was also proved by the TEM and nitrogen adsorption discussed below.

Figure 3a shows a TEM image of the SBA-1 submicrometer spheres, and the foamlike interior structure is clearly visible. In the high-resolution TEM image (Figure 3b), the mesopores of the SBA-1 mesostructure could be observed and it is interesting to see that, within the entire sphere, the alignment of mesopores kept well long-range order, exhibiting a single-crystal-like feature. The TEM images of the drumlike SBA-1 particles with different facets exposed to the electron beam are shown in Figures 3c and 3e, in which the foamlike inner texture was clearly seen. As shown in Figures 3d and 3f, the mesopores exhibited same alignment within the entire particle, indicating the single-crystal property of the drumlike SBA-1 particles. Note that the high-resolution TEM images of Figures 3d and 3f were obtained with the drumlike particles whose thickness was generally >1 μm; the periodicity of the mesopores in the TEM image would not be as beautiful as that of a sliced specimen. We also performed TEM observation with the grinded SBA-1 samples and it is also noteworthy that the SBA-1 particles possess a high degree of periodicity over a relatively large domain (see Figure 4). It could be concluded that the SBA-1 particles with well-defined morphology remained single-crystal-like, although they had foamlike interior textures.

The nitrogen adsorption−desorption isotherms and pore size distribution curves (calculated from the adsorption branch) of the single-crystal-like SBA-1 synthesized with different amounts of PAA are shown in Figure 5, and they all exhibited Type IV isotherms with three distinct adsorption steps at relative pressures (p/p_0) of 0.3−0.5, 0.75−0.95, and 0.95−0.99, respectively. The first step corresponded to nitrogen capillary condensation in the cagelike mesopores of SBA-1, and resulted in relatively narrow peaks (~3 nm) in the pore size distribution curves. It is necessary to indicate that the SBA-1 has an ordered 3D mesostructure with two types of globular cages, which possess slightly different pore sizes.[19] The peak at ~3 nm was due to the overlap of the two types of global cagelike mesopores. The second adsorption step at p/p_0 = 0.75−0.95 resulted in a broad pore size distribution centered at 20, 25, 27, and 28 nm, respectively, depending on the PAA amount, corresponding to

Table 1. Structural Parameters of the Calcined SBA-1 Samples Synthesized with Different Amounts of PAA

sample[a]	d_{210} (nm)	BET surface area ($m^2\ g^{-1}$)	mesopore size (nm)	nanopore size (nm)	pore volume ($cm^3\ g^{-1}$)
SBA-1-4	5.0	497	3.0	20, 62	1.09
SBA-1-5	5.0	459	3.1	25, 68	1.15
SBA-1-6	5.1	388	3.1	27, 79	1.15
SBA-1-7.5	5.2	443	3.1	28, 121	1.39

[a] The suffix number indicates the amount of PAA used in the synthesis.

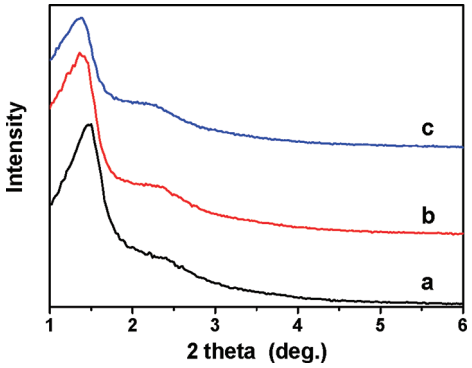

Figure 6. X-ray diffraction (XRD) patterns of the calcined SBA-1 samples prepared with different amounts of 1,3,5-TMB (0.18 g (pattern a), 0.36 g (pattern b), and 0.72 g (pattern c)).

the secondary interstitial multicellular nanopores, as observed in the SEM and TEM images. The third adsorption step at p/p_0 = 0.95−0.99 is noteworthy. In the N_2 adsorption isotherm of nanoparticles, an adsorption step usually appeared at p/p_0 values up to 0.95, which could be attributed to the voids between the packed nanoparticles.[20] However, here, in our case, the sizes of the SBA-1 particles were submicrometer or even in the range of several micrometers, so the adsorption step at p/p_0 = 0.95−0.99 could not be attributed to the voids of stacked particles. In the SEM (Figure S5 in the Supporting Information) and TEM images (see Figure 3) of the SBA-1 particles, larger nanopores with pore sizes of ∼100 nm could be observed. The third adsorption step could then be attributed to larger nanopores inside the SBA-1 particles, and in the pore size distribution curves (Figure 5B), they gave rise to another broad peak centered at 62, 68, 79, and 121 nm, respectively, depending on the amount of PAA. The mesostructure and pore parameters of the SBA-1 samples are listed in Table 1. Although there appeared three peaks in the pore size distribution curves, the latter two larger pores were ascribed to the secondary nanopores inside the SBA-1 particles.

The pore size distribution curves could also be calculated with the desorption branch of the isotherms. In some cases, due to the Tensile Strength Effect (TSE) phenomenon presented in the desorption branch, the pore size distribution derived from the desorption branch showed artificial peaks.[21] Here, in our case, the pore size distribution curves calculated from the desorption branch (see Figure S6 in the Supporting Information) also displayed a bimodal pore size distribution, and these results further proved the hierarchically porous nature of these materials.

The mesopores were templated by the CPC surfactant micelles. The secondary nanopores were templated by the PAA domains with

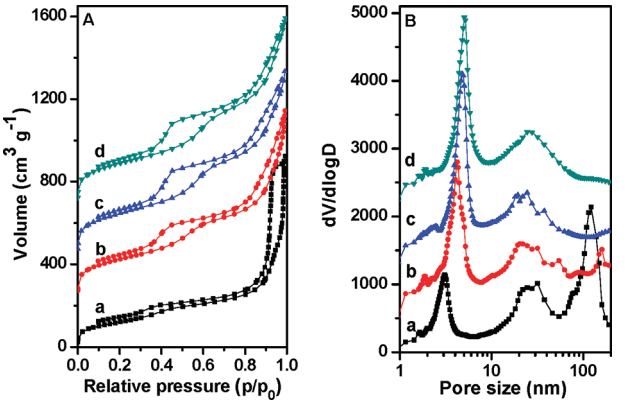

Figure 7. (A) Nitrogen adsorption−desorption isotherms and (B) pore size distribution curves of the calcined SBA-1 samples prepared with different amounts of 1,3,5-TMB (0 g (curve a), 0.18 g (curve b), 0.36 g (curve c), and 0.72 g (curve d)).

different sizes, which were extruded and phase-separated from the PAA/CPC complex, because of the co-assembly between the silica precursors and the CPC micelles. With the addition of more PAA in the synthesis, a larger amount of phase-separated PAA would induce larger domain size and result in larger secondary nanopores (see Table 1). Meanwhile, the presence of more and larger secondary nanopores within the SBA-1 particles would gradually impact the long-range order of the SBA-1 mesostructure, thus resulting in less-resolved XRD patterns, as shown in Figure 1.

Among several three-dimensional (3-D) cubic mesophase materials, SBA-1 is an interesting material and possesses a cage-type structure with 3-D interconnected small open windows.[19] However, it was found that the synthesis of SBA-1 required a low temperature of 273 K under acidic conditions, and the cubic mesophase underwent a phase transformation to the hexagonal mesophase when the synthesis temperature was above 313 K.[22] Recently, Ting et al. demonstrated a successful synthesis of SBA-1 under highly acidic conditions at the temperature up to 100 °C with sugars as auxiliary agents.[23] Here, in our work with the PAA/surfactant mesomorphous complexes as a template, SBA-1 could be facilely fabricated under weakly basic conditions, and the synthesis temperature could be as high as 120 °C.[11] To our knowledge, this is the highest synthesis temperature for SBA-1.

The incorporation of alkanes as swelling agents was an effective method to enlarge the pore size of mesoporous silica.[24] To expand the size of the ordered mesopore of SBA-1 particles, 1,3,5-trimethylbenzene (TMB) was used as an organic swelling agent in the synthesis with 7.5 g of PAA. The X-ray diffraction (XRD) patterns (see Figure 6) of the calcined products synthesized with different amounts of 1,3,5-TMB indicated that, with the addition of more 1,3,5-TMB, the *d*-spacing was gradually increased, and the originally resolved peaks (Figure 1d) become broadened and merged together. The N_2 adsorption−desorption isotherms and pore size distribution curves of the samples synthesized with 1,3,5-TMB are shown in Figure 7. It was observed that size of the cagelike mesopore of the SBA-1 was gradually increased from 3.1 nm to 5.0 nm, and BET surface area were increased from 443 m^2/g to 693 m^2/g with the addition of 1,3,5-TMB (see Table 2).

The morphology of the sample synthesized with the addition of 1,3,5-TMB remained almost unchanged, as shown in Figure S7 in the Supporting Information. From a broken particle, the inner

dx.doi.org/10.1021/cm2017856 |*Chem. Mater.* 2011, 23, 4241–4249

Table 2. Structural Parameters of the Calcined SBA-1 Samples Synthesized with Different Amounts of 1,3,5-TMB[a]

sample[b]	d_{210} (nm)	BET surface area ($m^2\ g^{-1}$)	mesopore size (nm)	nanopore size (nm)	pore volume ($cm^3\ g^{-1}$)
SBA-1	5.2	443	3.1	28, 121	1.39
SBA-1-TMB-0.18	6.1	640	4.2	28, 160	1.34
SBA-1-TMB-0.36	6.3	718	4.8	28, —	1.35
SBA-1-TMB-0.72	6.4	693	5.0	28, —	1.35

[a] The amount of PAA was kept at 7.5 g. [b] The suffix number indicates the amount of 1,3,5-TMB used in the synthesis.

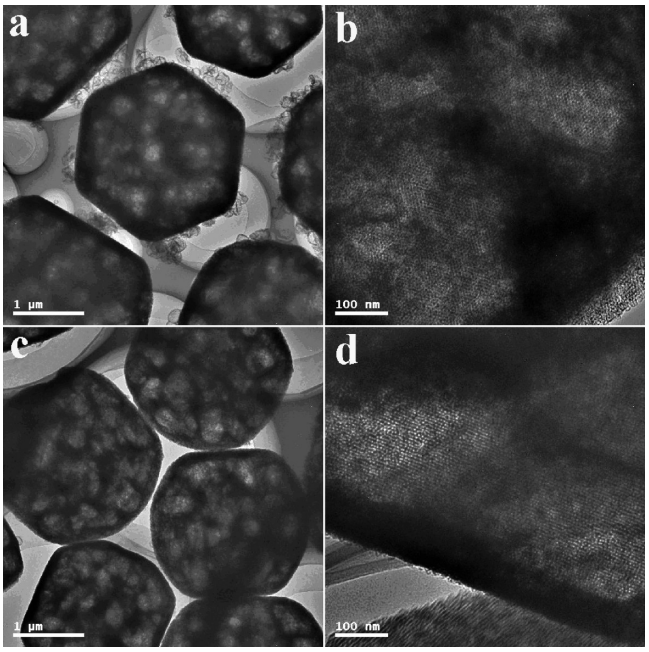

Figure 8. TEM images of the calcined SBA-1 samples synthesized with (a, b) 0.18 g of 1,3,5-TMB and (c, d) 0.72 g of 1,3,5-TMB.

nanopores were enlarged to several hundreds of nanometers (Figure S7b in the Supporting Information). The TEM images of the calcined SBA-1 synthesized with the addition of 1,3,5-TMB are shown in Figure 8. The alignment of the mesopores still maintained good long-range order within the particle and the foamlike secondary nanopores became more pronounced. This means that the addition of 1,3,5-TMB not only swelled the surfactant micelles to enlarge the mesopores, but also swelled the PAA phase with the aid of CPC surfactant to enlarge the domain size for the secondary nanopores. Based on TEM images, some of the secondary nanopores were around hundreds of nanometers in size, and the large pore size could go beyond the detection limit of the N_2 adsorption measurements. This could explain why, in the pore size distribution curves (see Figure 7B) after the addition of 0.18 g of 1,3,5-TMB, the peak of the larger secondary nanopore increased to 160 nm. Whereas with further increases in the amount of 1,3,5-TMB, there appeared only one peak of the secondary nanopore but with broader distribution. The broadened XRD patterns could also be attributed to the enlargement of the secondary nanopores within the SBA-1 particles.

Inspired by the successful fabrication of single-crystal-like, hierarchically nanoporous silica SBA-1, using the template of the organic mesomorphous complexes of PAA and CPC, we expand the method to synthesize PMO materials with the organic silica precursors of BTEE. The PAA and CPC complexes were finally removed by solvent extraction. By varying the amount of BTEE

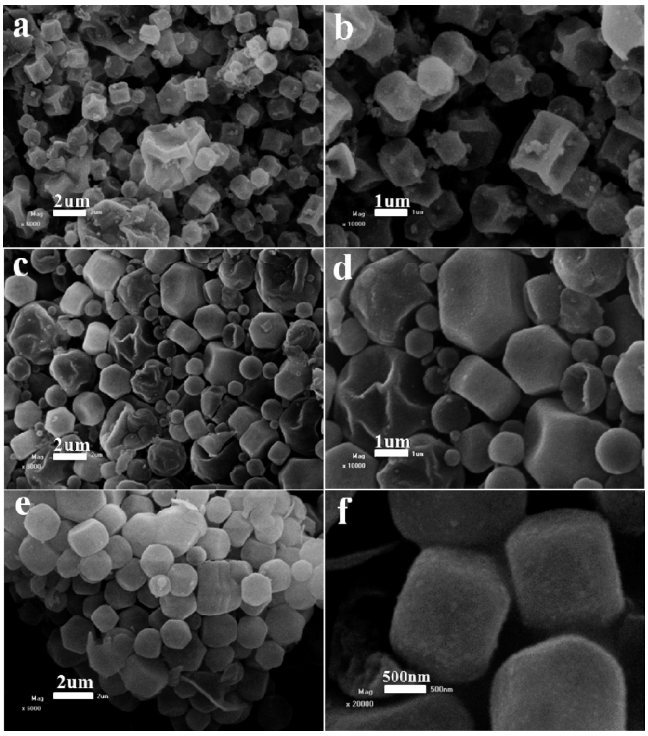

Figure 9. SEM images of the as-synthesized H-PMO samples obtained with different amounts of BTEE ((a, b) 1.8 g, (c, d) 2.7 g, and (e, f) 3.6 g).

(from 1.8 g to 3.6 g), a series of PMO with tunable morphologies was fabricated. Figure 9 shows the SEM images of the as-synthesized PMO synthesized at 1.8, 2.7, and 3.6 g of BTEE. It can be seen that all three samples exhibited hexagonal morphology similar to that of SBA-1-7.5. Interetstingly, as the amount of BTEE increased, the morphology of the samples evolved from hollow particles to solid particles. Some representative SEM images from different viewpoint are also shown in Figure S8 in the Supporting Information.

Upon the addition of BTEE, it would permeate into the colloidal PAA/CPC complex template and meanwhile undergo hydrolysis. With relatively smaller amounts of BTEE, it could only permeate and react with the outer layer of the PAA/CPC template, and then hollow PMO particles were obtained. However, with larger amounts of BTEE, more organosilane precursors penetrated totally inside the colloidal PAA/CPC complex and underwent hydrolysis to form solid PMO particles. Figure 10 shows the SAXS patterns of the three extracted PMO samples. For the sample with 3.6 g of BTEE, three diffraction peaks were clearly observed and they were indexed to the (200), (210), and (211) characteristic diffractions of the cubic $Pm\bar{3}n$ mesostructure. As the amount of BTEE decreased, the diffraction peaks exhibited were less resolved and the three peaks appeared only as

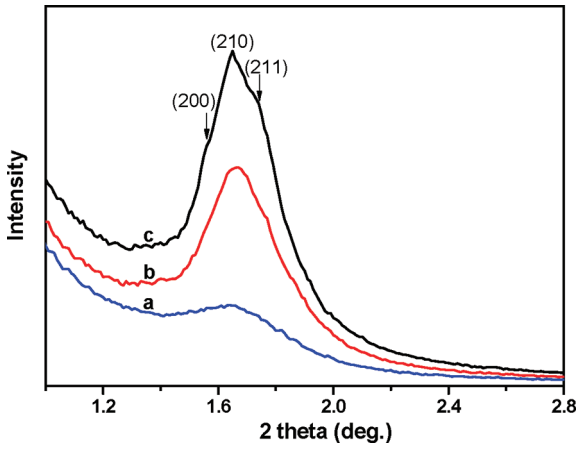

Figure 10. SAXS patterns of the solvent-extracted H-PMO samples obtained with different amounts of BTEE (1.8 g (pattern a), 2.7 g (pattern b), and 3.6 g (pattern c)).

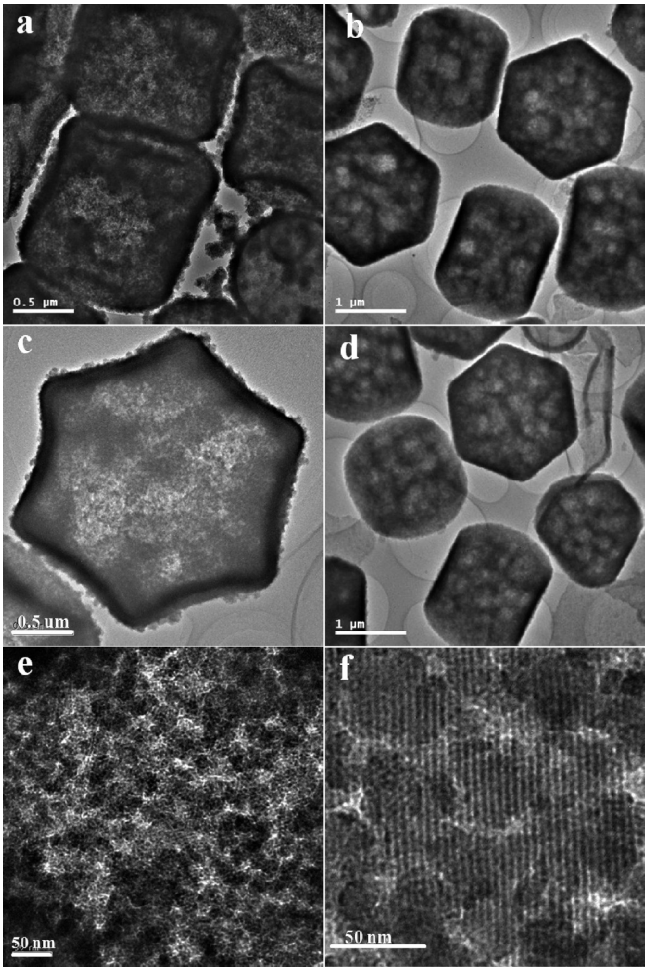

Figure 11. TEM images of the solvent-extracted H-PMO samples obtained with different amounts of BTEE ((a, c, e) 1.8 g and (b, d, f) 3.6 g).

a broad peak. TEM images (Figure 11) of the PMO synthesized with 1.8 g of BTEE exhibited a hollow structure with well-defined morphology corresponding to the SEM images. The mesopores

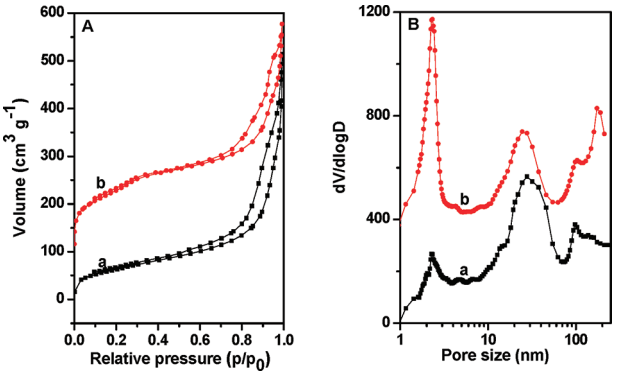

Figure 12. (A) Nitrogen adsorption−desorption isotherms and (B) pore size distribution of the solvent-extracted H-PMO samples obtained with different amounts of BTEE (1.8 g (curve a) and 3.6 g (curve b)).

Table 3. Structural Parameters of the Solvent-Extracted HPMO Samples Obtained with Different Amounts of BTEE

sample[a]	BET surface area ($m^2\ g^{-1}$)	mesopore size (nm)	nanopore size (nm)	pore volume ($cm^3\ g^{-1}$)
H-PMO-1.8	229	2.28	28, 100	0.71
H-PMO-3.6	466	2.28	25, 100	0.71

[a] The suffix number indicates the amount of BTEE used in the synthesis.

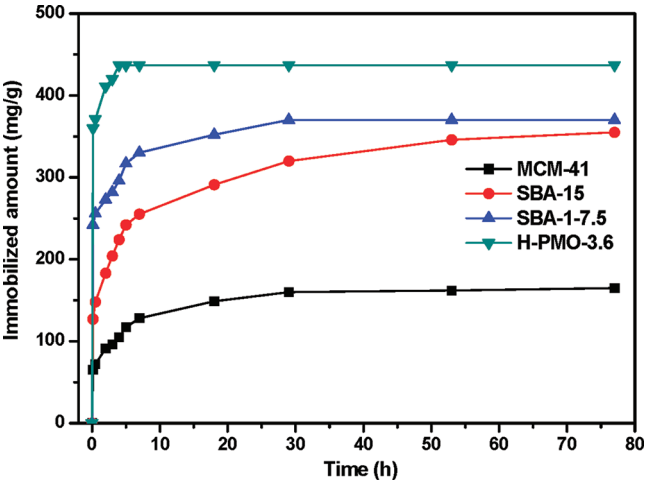

Figure 13. Comparison of the lysozyme immobilization rate on different materials, as a function of time.

were not well-ordered, as indicated by the SAXS pattern (see Figure 10a). For the PMO synthesized with 3.6 g of BTEE, the foamlike inner feature of the particles as well as an ordered alignment of mesopores through the entire particle can be observed (see Figure 11). Nitrogen adsorption isotherms and pore size distribution curves of the extracted PMO samples (see Figure 12) exhibited the feature of mesopores and very broad secondary nanopores. It is noteworthy that, with the increase of the amount of BTEE from 1.8 g to 3.6 g, the adsorption step of 0.3−0.5 became pronounced and the BET surface area increased from 229 $m^2\ g^{-1}$ to 446 $m^2\ g^{-1}$ (see Table 3). Based on the above results, hierarchically nanoporous PMO materials with well-defined morphology have

dx.doi.org/10.1021/cm2017856 |*Chem. Mater.* 2011, 23, 4241–4249

Table 4. Enzyme Properties and Immobilized Amounts on Siliceous Particles with Different Porosity

				Enzyme Immobilized Amount (mg g^{-1})			
	molecular weight, M_w (kDa)	size	isoelectric point, PI	MCM-41	SBA-15	SBA-1−7.5	H-PMO-3.6
lysozyme	14.6	19 Å × 25 Å × 43 Å	11	165	379	370	437
BSA	69	40 Å × 40 Å × 140 Å	4.7	64	162	320	402

been fabricated with the PAA/CPC mesomorphous complex as a template.

In order to study the bioimmobilization ability of the hierarchically nanoporous SBA-1 and H-PMO, SBA-1-7.5 and H-PMO-3.6 were used as typical examples in the immobilization of lysozyme and BSA. Previous studies have shown that the bimodal porous structure of the silica materials had significant influence on the bioimmobilization process.[25] Herein, the SBA-15 (pore size of 7 nm and pore volume of 1.01 $cm^3 g^{-1}$) and MCM-41 (pore size of 2.7 nm and pore volume of 0.79 $cm^3 g^{-1}$) were chosen as the reference samples. Figure 13 presented the adsorption kinetics of MCM-41, SBA-15, SBA-1-7.5, and H-PMO-3.6 in 0.5 mg mL^{-1} lysozyme solution and the immobilized amount of lysozyme from four samples are summarized in Table 4. It is shown that both the SBA-1-7.5 and H-PMO-3.6 exhibited a rapid adsorption rate with saturation times of 29 and 4 h, respectively, which were greatly shorter than that for MCM-41 (3 days) and SBA-15 (5 days). The maximum adsorption amounts for the four samples were measured to be 370, 437, 165, and 379 mg g^{-1}, respectively. For MCM-41, the driving force for the immobilization was mainly due to the electrostatic interaction, since the pore size of MCM-41 was only 2.5 nm, which was smaller than the size of lysozyme, leading to slow adsorption kinetics and a smaller adsorption amount. For SBA-15 and SBA-1-7.5, the maximum adsorption amounts of the two samples were measured to be equivalent; however, the SBA-1-7.5 showed a more rapid adsorption rate (29 h vs 5 days). Although SBA-15 had a larger pore size of 7 nm, which was big enough to host lysozyme, the hierarchically nanoporous structure of the SBA-1-7.5 was favorable to faster diffusion of the lysozyme. However, for H-PMO-3.6, the hierarchically nanoporous structure, as well as the inherent hydrophobic bridged-ethylene groups, contributed to a high maximum adsorption amounts and a rapid adsorption rate. To further survey the adsorption performance of the materials, BSA was chosen as a protein example, since BSA has a larger molecular size (40 Å × 40 Å × 140 Å) than lysozyme (19 Å × 25 Å × 43 Å). Table 4 summarizes the immobilized amount of BSA of the four samples. Approximately 320 mg g^{-1} BSA was immobilized onto SBA-1-7.5, and this value was greatly larger than that on MCM-41 (64 mg g^{-1}) and SBA-15 (162 mg g^{-1}). The higher immobilized amounts on SBA-1-7.5 were attributed to the hierarchical pore structure. Notably, the H-PMO-3.6 had the highest immobilized amount of BSA (402 mg g^{-1}). This is due to the fact that PMO has not only a hierarchically nanoporous structure but also uniformly distributed bridged-ethylene groups that provide a hydrophobic surface. It is concluded that the H-PMO could serve as a promising candidate in the immobilization of larger biomolecules.

CONCLUSION

With the organic mesomorphous complexes of poly(acrylic acid) (PAA)) and cationic surfactant (hexadecylpyridinium chloride (CPC)) as templates, single-crystal-like, hierarchically nanoporous silica SBA-1 particles were successfully fabricated. By adjusting the amounts of PAA in the synthesis, a series of silica particles with well-defined morphologies and well-ordered cubic $Pm\bar{3}n$ mesostructure were obtained. Both the mesostructure and well-defined morphology of the silica particles inherited those of the corresponding PAA/CPC mesomorphous complexes. The materials possess hierarchically nanopores that correspond to the mesopore size of SBA-1 templated by surfactant micelles and secondary interstitial nanopores templated by phase-separated PAA, respectively. Notably, the presence of a large amount of foamlike secondary nanopores did not disturb the single-crystal characteristic of the SBA-1 particles. By means of pore-expanding with 1,3,5-trimethylbenzene, the mesopore size of the SBA-1 could be easily tuned from 3.1 nm to 5.0 nm, while the morphology of the particles was not changed. Moreover, a series of ethylene-bridged H-PMO with well-defined morphology were fabricated. Because of the hierarchical structure and hydrophobic surface property, the H-PMO showed a superior adsorption capacity and rapid adsorption dynamics. Because there are many types of polyelectrolytes and oppositely charged surfactants, the synthesis method with polyelectrolyte/surfactant mesomorphous complexes as a template can be regarded as a general method to fabricate hierarchically porous materials and different mesostructures, and new morphologies are expected.

ASSOCIATED CONTENT

Supporting Information. This material is available free of charge via the Internet at http://pubs.acs.org.

AUTHOR INFORMATION

Corresponding Author
*E-mail address: chenth@nankai.edu.cn.

ACKNOWLEDGMENT

This work was supported by National Science Foundation of China (Grant Nos. 20873070, 20973095), National Basic Research Program of China (No. 2009CB623502), and NCET of Ministry of Education (No. NCET-07-0448) and MOE (No. IRT-0927).

REFERENCES

(1) (a) Kuang, D.; Brezesinski, T.; Smarsly, B. *J. Am. Chem. Soc.* **2004**, *126*, 10543. (b) Sel, O.; Kuang, D.; Thommes, M.; Smarsly, B. *Langmuir* **2006**, *22*, 2311.
(2) Zhao, B.; Collinson, M. *Chem. Mater.* **2010**, *22*, 4312.
(3) (a) Sen, T.; Tiddy, G. J. T.; Casci, J. L.; Anderson, M. W. *Angew. Chem., Int. Ed.* **2003**, *42*, 4649. (b) Stein, A.; Li, F.; Denny, N. R. *Chem. Mater.* **2008**, *20*, 649.
(4) (a) Rathod, S. B.; Ward, T. L. *J. Mater. Chem.* **2007**, *17*, 2329. (b) Guo, X.; Deng, Y.; Tu, B.; Zhao, D. *Langmuir* **2010**, *26*, 702.
(5) (a) Nakanishi, K.; Tanaka, N. *Acc. Chem. Res.* **2007**, *40*, 863. (b) Niu, D.; Ma, Z.; Li, Y.; Shi, J. *J. Am. Chem. Soc.* **2010**, *132*, 15144.
(6) (a) Zhang, H.; Hardy, G. C.; Khimyak, Y. Z.; Rosseinsky, M. J.; Cooper, A. I. *Chem. Mater.* **2004**, *16*, 4245. (b) Wang, J.; Xiao, Q.; Zhou,

H.; Sun, P.; Yuan, Z.; Li, B.; Ding, D.; Shi, A.; Chen, T. *Adv. Mater.* **2006**, *18*, 3284.
(7) Meldrum, F. C.; Cölfen, H. *Chem. Rev.* **2008**, *108*, 4332.
(8) Mann, S. *Biomineralization: Principles and Concepts in Bioinorganic Materials Chemistry*; Oxford University Press: NewYork, 2001.
(9) (a) Antonietti, M.; Conrad, J. *Angew. Chem., Int. Ed.* **1994**, *33*, 1869. (b) Faul, C. F. J.; Antonietti, M. *Adv. Mater.* **2003**, *15*, 673. (c) Piculell, L.; Norrman, J.; Svensson, A.; Lynch, I.; Bernardes, J. S.; Loh, W. *Adv. Colloid Interface Sci.* **2009**, *147*−*148*, 228. (d) Zhou, S.; Chu, B. *Adv. Mater.* **2000**, *12*, 545. (e) von Ferber, C.; Löwen, H. *Faraday Discuss.* **2005**, *128*, 389. (f) Ikkala, O.; ten Brinke, G. *Chem. Commun.* **2004**, *19*, 2131. (g) Macknight, W. J.; Ponomarenko, E. A.; Tirrell, D. A. *Acc. Chem. Res.* **1998**, *31*, 781.
(10) Yang, B.; Edler, K. *Chem. Mater.* **2009**, *21*, 1221.
(11) Wang, J.; Zhou, H.; Sun, P.; Ding, D.; Chen, T. *Chem. Mater.* **2010**, *22*, 3829.
(12) (a) Inagaki, S.; Guan, S.; Fukushima, Y.; Ohsuna, T.; Terasaki, O. *J. Am. Chem. Soc.* **1999**, *121*, 9611. (b) Asefa, T.; MacLachlan, M. J.; Coombs, N.; Ozin, G. A. *Nature* **1999**, *402*, 867. (c) Lee, H.; Kim, J. M.; Stucky, G. D. *J. Am. Chem. Soc.* **2009**, *131*, 14249. (d) Li, J.; Wei, Y.; Deng, Y.; Gu, D.; Yang, X.; Zhang, L.; Tu, B.; Zhao, D. *J. Mater. Chem.* **2010**, *20*, 6460. (e) Kruk, M.; Mandal, M. *J. Phys. Chem. C* **2010**, *114*, 20091. (f) Jeong, E. Y.; Burri, A.; Lee, S. Y.; Park, S. E. *J. Mater. Chem.* **2010**, *20*, 10869. (g) Wang, W.; Lofgreen, J.; Ozin, G. A. *Small* **2010**, *6*, 2634.
(13) (a) Park, M.; Park, S. S.; Selvaraj, M. *J. Porous Mater.* **2011**, *18*, 217. (b) Park, M.; Park, S. S.; Selvaraj, M. J.; Zhao, D.; Ha, C. K. *Microporous Mesoporous Mater.* **2009**, *124*, 76. (c) Qiao, S. Z.; Yu, C. Z.; Xing, W.; Hu, Q. H.; Djojoputro, H.; Lu, G. Q. *Chem. Mater.* **2005**, *17*, 6172.
(14) Zhou, Z.; Taylor., R. N. T.; Kullmann, S.; Bao, H.; Hartmann, M. *Adv. Mater.* **2011**, *23*, 2627.
(15) Wu, Z.; Zhao, D. *Chem. Commun.* **2011**, *47*, 3332.
(16) (a) Zhao, D.; Feng, J.; Huo, Q.; Melosh, N.; Fredrickson, G. H.; Chmelka, B. F.; Stucky, G. D. *Science* **1998**, *279*, 548. (b) Zhang, Q. H.; Lu, F.; Li, C. L.; Wang, Y.; Wan, H. L. *Chem. Lett.* **2006**, *35*, 190.
(17) Miyasaka, K.; Han, L.; Che, S.; Terasaki, O. *Angew. Chem., Int. Ed.* **2006**, *45*, 6516.
(18) Leonard, M.; Strey, H. H. *Macromolecules* **2010**, *43*, 4379.
(19) (a) Huo, Q.; Margolese, D. I.; Ciesla, U.; Feng, P.; Gier, T. E.; Sieger, P.; Leon, R.; Petroff, P. M.; Schüth, F.; Stucky, G. D. *Nature* **1994**, *368*, 317. (b) Huo, Q.; Leon, R.; Petroff, P. M.; Stucky, G. D. *Science* **1995**, *268*, 1324.
(20) (a) Wang, J.; Xiao, Q.; Zhou, H.; Sun, P.; Ding, D.; Chen, T. *J. Colloid Interface Sci.* **2008**, *323*, 332. (b) Han, L.; Chen, Q.; Wang, Y.; Gao, C.; Che, S. *Microporous Mesoporous Mater.* **2011**, *139*, 94.
(21) Groen, J. C.; Peffer, L. A. A.; Pérez-Ramírez, J. *Microporous Mesoporous Mater.* **2003**, *60*, 1.
(22) Kim, M. J.; Ryoo, R. *Chem. Mater.* **1999**, *11*, 487.
(23) Ting, C. C.; Wu, H. Y.; Pan, Y. C.; Vetrivel, S.; Fey, G. T. K.; Kao, H. M. *J. Phys. Chem. C* **2010**, *114*, 19322.
(24) (a) Beck, J. S. U.S. Patent 5,057,296, 1991. (b) Suteewong, T.; Sai, H.; Cohen, R.; Wang, S.; Bradbury, M.; Baird, B.; Gruner, S.; Wiesner, U. *J. Am. Chem. Soc.* **2011**, *133*, 172. (c) Mizutani, M.; Yamada, Y.; Nakamura, T.; Yano, K. *Chem. Mater.* **2008**, *20*, 4777.
(25) Wang, Y.; Caruso, F. *Chem. Mater.* **2005**, *17*, 953.